


# Distinguishing pancreatic solid serous cystadenomas from nonfunctional pancreatic neuroendocrine tumors by computed tomography

## A propensity score analysis

Xu Fang, MS<sup>a</sup>, Hui Jiang, MD<sup>b</sup>, Kai Cao, MD<sup>a</sup>, Jing Li, MD<sup>a</sup>, Fang Liu, MS<sup>a</sup>, Li Wang, MD<sup>a</sup>, Jianping Lu, MD<sup>a</sup>, Chengwei Shao, MD<sup>a</sup>, Yun Bian, MD<sup>a,\*</sup> 

### Abstract

This study aims to evaluate the utility of calculated computed tomography (CT) attenuation value ratio (AVR) and enhancement pattern in distinguishing pancreatic solid serous cystadenomas (SCAs) from nonfunctional pancreatic neuroendocrine tumors (NF-pNETs). A total of 142 consecutive patients with 22 solid SCAs and 120 NF-pNETs confirmed by pathology were included in this retrospective study. All patients underwent preoperative contrast-enhanced CT and were categorized into 2 groups, solid SCA and NF-pNET groups. Patients with NF-pNETs were matched to patients with solid SCAs via propensity scores. AVR was measured and defined as: attenuation value of tumor/attenuation value of normal pancreas. AVR and enhancement pattern performance were assessed according to the discriminative abilities of patients. After matching, 29 patients were allocated to the NF-pNET group. Before matching, sex, age, and the peak enhanced value phase were significantly different between solid SCA and NF-pNET patients ( $P < .05$ ). After matching, no significant difference was observed between both groups ( $P > .05$ ). Solid SCAs AVRs were significantly smaller than NF-pNETs AVRs in all unenhanced, arterial, portal venous, and delayed phases ( $P < .05$ ). Solid SCAs showed significantly more wash-in and wash-out enhancement patterns than NF-pNETs ( $P < .05$ ). For unenhanced, arterial, portal venous, and delayed phases, and enhancement pattern, the area under the curve (AUC) values were 0.96, 0.72, 0.80, 0.85, and 0.86, respectively. Low AVR on unenhanced CT and wash-in and wash-out enhancement patterns were useful for differentiating solid SCAs from NF-pNETs and may be useful for clinical decisions, a clearer opinion will be formed with further studies to be conducted with larger patient numbers.

**Abbreviations:** AUC = area under the curve, AVR = attenuation value ratio, CI = confidence interval, CT = computed tomography, MRI = magnetic resonance imaging, NF-pNETs = nonfunctional pancreatic neuroendocrine tumors, PSM = propensity score matching, ROI = regions of interest, SCAs = serous cystadenomas, WHO = World Health Organization.

**Keywords:** cystadenoma, neuroendocrine tumors, pancreas, serous, tomography, X-ray computed

## 1. Introduction

The incidental detection of cystic and solid pancreatic lesions has increased with the widespread and frequent use of cross-sectional imaging. Solid serous cystadenomas (SCAs) are significantly often misdiagnosed as nonfunctioning pancreatic neuroendocrine tumors (NF-pNETs) and then treated using unnecessary surgical resection.<sup>[1,2]</sup> Pancreas solid SCAs and NF-pNETs are significantly different in terms of tumor aggressiveness, treatment, and prognosis. Therefore, a distinction between these 2 is essential. Solid SCAs are benign, but

NF-pNETs are potentially malignant, with a 5-year survival rate of 51.3%.<sup>[3]</sup> Moreover, the treatment for these tumors is different. Solid SCAs should be followed up for 1 year and require no follow-up if asymptomatic, and surgery is recommended only in patients with symptoms related to adjacent organ compression.<sup>[4,5]</sup> However, NF-pNETs need extended resection in combination with other treatments, such as adjuvant chemotherapy or radiotherapy, to be treated.<sup>[6]</sup> Therefore, a preoperative differentiation method between solid SCAs and NF-pNETs is urgently needed as proper differentiation can have a crucial bearing on outcomes.

This work was supported in part by the National Science Foundation for Scientists of China (81871352, 82171915, and 82171930), The Natural Science Foundation of Shanghai Science and Technology Innovation Action Plan (21ZR1478500, 21Y11910300), Clinical Research Plan of SHDC (SHDC2020CR4073), and 234 Platform Discipline Consolidation Foundation Project (2019YPT001, 2020YPT001).

The authors have no conflicts of interest to disclose.

All data generated or analyzed during this study are included in this published article [and its supplementary information files].

<sup>a</sup> Department of Radiology, Changhai Hospital of Shanghai, Naval Medical University, Shanghai, China, <sup>b</sup> Department of Pathology, Changhai Hospital of Shanghai, Naval Medical University, Shanghai, China.

\*Correspondence: Yun Bian, Department of Radiology, Changhai Hospital of Shanghai, Naval Medical University, Changhai Road 168, Shanghai 200434, China (e-mail: bianyun2012@foxmail.com).

Copyright © 2022 the Author(s). Published by Wolters Kluwer Health, Inc. This is an open-access article distributed under the terms of the Creative Commons Attribution-Non Commercial License 4.0 (CCBY-NC), where it is permissible to download, share, remix, transform, and build up the work provided it is properly cited. The work cannot be used commercially without permission from the journal.

How to cite this article: Fang X, Jiang H, Cao K, Li J, Liu F, Wang L, Lu J, Shao C, Bian Y. Distinguishing pancreatic solid serous cystadenomas from nonfunctional pancreatic neuroendocrine tumors by computed tomography: A propensity score analysis. *Medicine* 2022;101:37(e30523).

Received: 12 July 2021 / Received in final form: 7 August 2022 / Accepted: 8 August 2022

<http://dx.doi.org/10.1097/MD.00000000000030523>

Endoscopic ultrasonography-guided fine-needle aspiration is considered sensitive for pathological confirmation from tumor biopsy samples. However, endoscopic ultrasonography-guided fine-needle aspiration is invasive, expensive, and time-consuming, with a rather significant risk of complications.<sup>[7,8]</sup> Magnetic resonance imaging (MRI) is increasingly being used for identifying and characterizing pancreatic cystic neoplasms.<sup>[5]</sup> Studies have reported using MRI with clear characteristics for evaluating suspected solid SCAs, but solid SCAs were often significantly misdiagnosed as NF-pNETs by computed tomography (CT).<sup>[9–11]</sup> However, the research on differentiation of solid SCAs from NF-pNETs by CT is still limited. In this study, we have focused on multidetector CT, because there are still many patients with solid SCAs that are misdiagnosed as NF-pNETs by CT, lacking MRI or EUS examination.

In clinical research, the gold standard level of evidence is randomized controlled trials, and the availability of nonrandomized retrospective data is growing. However, a primary concern related to analyzing such data is the comparability of exposure groups with respect to confounding variables. Propensity score matching (PSM) aims to equate exposure groups with respect to measured baseline covariates to perform comparisons with reduced selection bias.<sup>[12,13]</sup> In addition, CT attenuation value is related to patient respiration, tube voltage, and CT scanners, among others.<sup>[14,15]</sup> To increase the accuracy of the measurements, we used the CT attenuation value ratio (AVR) of the tumor to normal pancreas. Using PSM, this retrospective study aimed to evaluate the diagnostic performance of the CT AVR and enhancement pattern for differentiating solid SCAs from NF-pNETs.

## 2. Methods

This retrospective cross-sectional study was reviewed and approved by the Biomedical Research Ethics Committee of our institution, and the requirement for patient consent was waived due to the retrospective nature of this study.

### 2.1. Patients

The patient selection process is shown in Figure 1. We screened the institutional database for the medical records of patients with histologically confirmed solid SCAs and NF-pNETs who underwent curative surgical resection from May 2011 to September 2019. Exclusion criteria were as follows: patients not evaluated by contrast-enhanced CT within 1 week preoperatively (n = 8), pancreatic lesions that could not be visualized in CT images (n = 1), other tumors in the pancreas (n = 2), and NF-pNETs patients had cystic degeneration (n = 21), because cystic degeneration definitely affects the CT attenuation value. Consequently, 142 consecutive patients – 22 with solid SCAs and 120 with NF-pNETs – were included in this cross-sectional study.

### 2.2. CT protocol

CT imaging was performed using 320-slice or 256-slice multidetector-row helical CT scanners (Aquilion ONE, Canon Medical Systems, Tokyo, Japan, and Brilliance iCT, Philips Healthcare, Cleveland, Ohio, respectively), with an unenhanced scan, followed by triple-phase abdomen contrast-enhanced

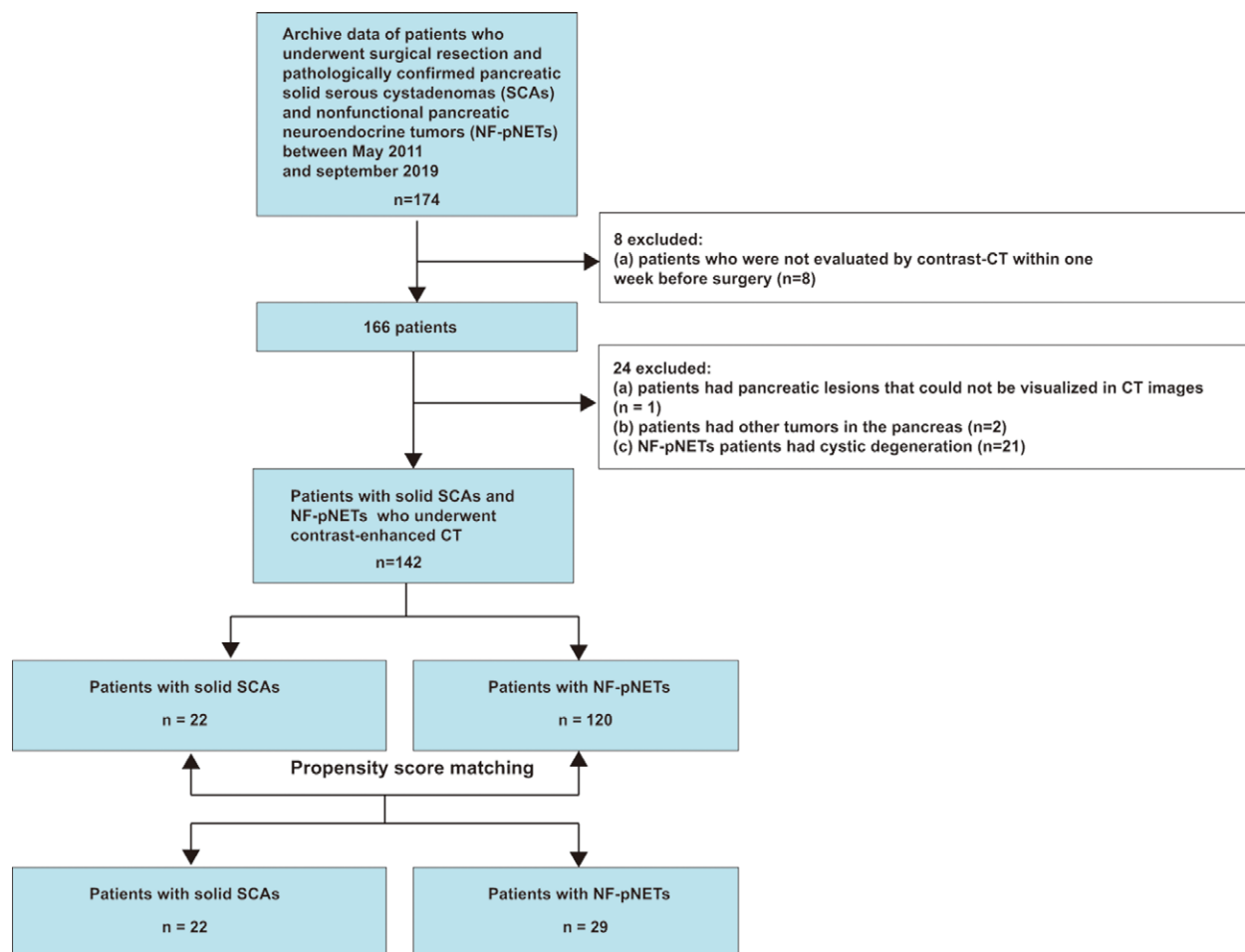


Figure 1. Flow diagram showing patient selection criteria.

scans. Tube voltage was 120 kV, tube current was 250 mA, and the rotation period was 0.5 seconds. Initially, a nonenhanced CT scan was performed, followed by a dynamic contrast-enhanced CT scan. The scan delay time was determined by the test bolus. Test bolus is a new method that can achieve better effect in abdominal examination. The optimal scan delay time was measured with a 15 to 20 mL of contrast agent. The test was performed in the abdominal aorta at the hilar level. According to the weight and age of the patients, the final scanning time was set as 3 to 5 seconds after the peak time obtained from the test, which was the time for data collection. The contrast agent (90–95 mL of 370 mgI/mL iopromide; Ultravist 370, Bayer Schering Pharma, Berlin, Germany) was injected at a rate of 4 to 5 mL/s with a power injector (Medrad Mark V plus, Bayer, Leverkusen, Germany) via the forearm vein, followed by 20 mL of normal saline for flushing. Images were obtained during arterial, portal venous, and delayed phases at 20 to 25 seconds, 60 to 70 seconds, and 110 to 130 seconds, respectively, after contrast medium injection. Slice thickness/scan and reconstruction intervals were 0.8/1.0 and 1.0/1.0 mm, respectively.

### 2.3. CT imaging analysis

Two abdominal radiologists with 10 years of experience retrospectively reviewed all CT images independently. These radiologists were blinded to patient clinical details and histopathological findings. In cases of discordance between both reviewers, a final decision was reached by consensus. The following CT imaging features were evaluated: tumor location, including the head, body, and tail of the pancreas; tumor size, which was defined as the maximal tumor diameter in an arterial phase cross-section; shape, that is, whether it is round or lobulated; main pancreatic duct dilation (>3 mm); tumor calcification; CT AVR, which is obtained using the density measured by placing regions of interest (ROI) on the tumor and the normal pancreas in every phase, followed by calculating tumor density divided by normal pancreas density; this parameter was measured by a radiologist. ROIs were placed both above the tumors and in the unaffected segments of the normal pancreas. The largest possible spherical ROI was used, excluding the pancreatic duct and partial volume averaging from extrapancreatic structures, as shown in Figure 2. The ROI attenuation value was measured 3 times and subsequently averaged; the peak enhanced value phase, which was defined as the largest tumor CT attenuation value in the enhanced phase; and enhancement pattern, that is, whether it is wash-in and wash-out, or persistent, or gradual. The wash-in and wash-out enhancement pattern was defined as the CT attenuation value of the tumor being stronger than that of the normal pancreas only in the arterial phase but equal to or smaller than that of the normal pancreas in portal venous and delayed phases. The persistent enhancement pattern was defined as the tumor CT attenuation value being stronger than the normal pancreas CT attenuation value in every enhanced phase. The gradual enhancement pattern was defined as the CT attenuation value of the tumor being less than that of the normal pancreas in the arterial phase but stronger than that of the normal pancreas in portal venous and delayed phases.

### 2.4. Clinical and pathologic data

Clinical data, including patient age, sex, and body mass index, were collected from medical records. The pathological diagnostic criteria for solid SCAs and NF-pNETs were based on the 2019 World Health Organization classification. The solid SCAs were composed of small back-to-back acini with no or minute central lumina and cytological features on histopathology and cells arranged in nests, sheets, and trabeculae separated by thick fibrous bands.<sup>[16]</sup>

### 2.5. Statistical analysis

Normal distribution and variance homogeneity tests were performed on all continuous variables. Continuous variables with a normal distribution was expressed as the mean values  $\pm$  standard deviation or as medians and interquartile ranges. To create a matched cohort of patients with NF-pNETs, a propensity score (logit model) was calculated for each patient based on the aforementioned baseline clinical variables, including age, sex, body mass index, tumor size, tumor location, shape, calcification, main pancreatic duct dilation, and peak enhancement. Matching was performed using a 1:2 matching protocol to select matched patients with NF-pNET without replacement (greedy-matching algorithm), with a caliper width of 0.2 of the standard deviation of the propensity score logit. We compared unmatched and matched variables between solid SCA and NF-pNET groups using the chi-square test, and Student *t* test or Kruskal–Wallis test. Moreover, Student *t* test or Kruskal–Wallis test was used to compare AVR. The diagnostic value of CT AVR of all lesions in every phase and the enhancement patterns for differentiating between solid SCAs and NF-pNETs were evaluated using a receiver operating characteristic analysis. The area under the curve (AUC) was also calculated.

A 2-tailed *P* value <.05 was considered statistically significant. Statistical analyses were performed with SPSS software version 25.0 (IBM Co., Armonk, NY, USA).

## 3. Results

### 3.1. Clinical and CT imaging features before and after matching

Clinical and CT imaging features of patients with solid SCAs and controlled NF-pNETs before and after PSM are shown in Table 1. Propensity score distributions in groups before and after matching are shown in Figure 3. In this study, a total of 22 patients with solid SCAs and 120 patients with NF-pNETs were included before matching. After matching, 29 pairs of patients were allocated to solid SCA and NF-pNET groups. Before matching, sex, age, calcification, and peak enhanced value phase were significantly different between solid SCA and NF-pNET groups (*P* < .05). After matching, no significant differences were found between solid SCA and NF-pNET groups (*P* > .05).



**Figure 2.** Graph showing the CT attenuation value measured by placing ROI on the tumor (black circle) and the normal pancreas (white circle). CT = computed tomography, ROI = regions of interest.

**Table 1**

**Clinical and CT imaging features of patients with solid serous cystadenomas and nonfunctional pancreatic neuroendocrine tumor before and after propensity score analysis.**

Characteristics	Before match			After match		
	Solid SCAs (n = 22)	NF-pNETs (n = 120)	P value	Solid SCAs (n = 22)	NF-pNETs (n = 29)	P value
Sex, n (%)			.007			.296
Male	6 (27.27)	70 (58.33)		6 (27.27)	12 (41.38)	
Female	16 (72.73)	50 (41.67)		16 (72.73)	17 (58.62)	
Age (yr, mean ± SD)	59.73 ± 11.64	54.16 ± 12.07	.029	59.73 ± 11.64	58.38 ± 9.04	.397
BMI (kg/m <sup>2</sup> , mean ± SD)	23.74 ± 2.50	22.72 ± 2.54	.063	23.74 ± 2.50	22.87 ± 2.16	.128
Size (mm, median, interquartile range)	26.50 ± 10.35	34.75 ± 24.09	.290	26.50 ± 10.35	30.38 ± 26.52	.336
Location, n (%)			.349			.657
Head	10 (45.45)	42 (35.00)		10 (45.45)	15 (51.72)	
Body and tail	12 (54.55)	78 (65.00)		12 (54.55)	14 (48.28)	
Shape, n (%)			.205			.861
Round	17 (77.27)	105 (87.50)		17 (77.27)	23 (79.31)	
Lobulated	5 (22.73)	15 (12.50)		5 (22.73)	6 (20.69)	
Calcification, n (%)			.037			.398
No	16 (72.73)	107 (89.17)		16 (72.73)	25 (86.21)	
Yes	6 (27.27)	13 (10.83)		6 (27.27)	4 (13.79)	
MPD, n (%)			.690			.938
Normal	20 (90.91)	102 (85.00)		20 (90.91)	25 (86.21)	
Dilation	2 (9.09)	18 (15.00)		2 (9.09)	4 (13.79)	
Phase of peak enhanced value n (%)			.003			1.000
Arterial phase	18 (81.82)	55 (45.83)		18 (81.82)	22 (75.86)	
Portal venous phase	4 (18.18)	39 (32.50)		4 (18.18)	6 (20.69)	
Delayed phase	0	26 (21.67)		0	1 (3.45)	

BMI = body mass index, CT = computed tomography, MPD = main pancreatic duct, NF-pNETs = nonfunctional pancreatic neuroendocrine tumors, SCAs = serous cystadenomas.

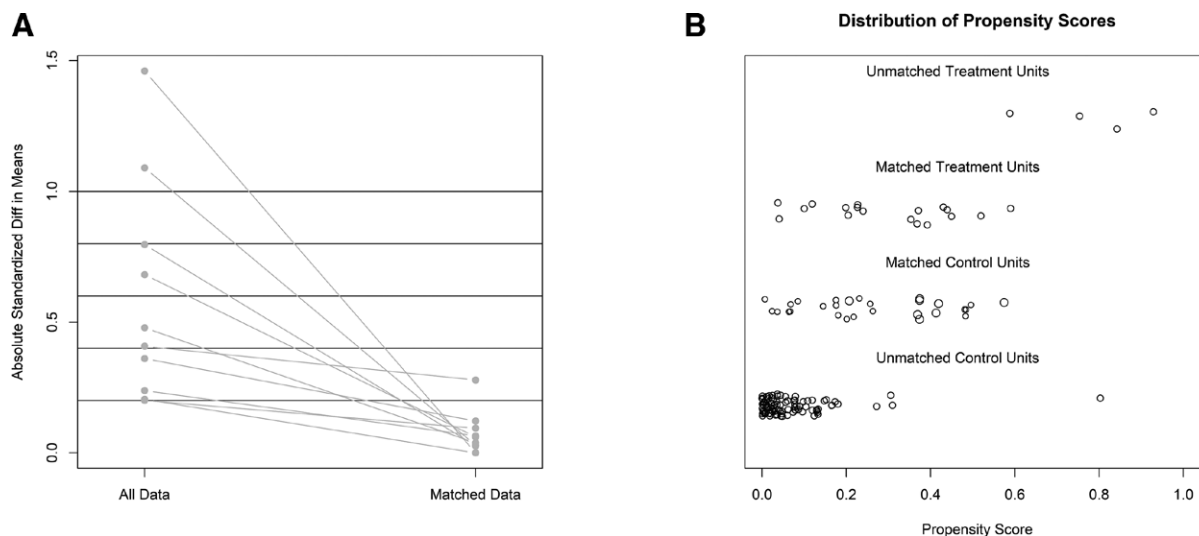


**Figure 3.** Baseline evaluation following propensity score matching. (A) Line plot of standardized differences before and after matching. (B) Dotplot of the distribution of propensity scores in matched and unmatched groups. The graph was produced using routines from the MatchIt package. PSM = propensity score matching.

**3.2. AVR and enhancement patterns**

Solid SCA AVRs were significantly smaller than NF-pNETs AVRs in all unenhanced, arterial, portal venous, and delayed phases ( $P < .05$ ). Solid SCAs and NF-pNETs AVRs in unenhanced and contrast-enhanced images are shown in Figure 4. None showed a gradual enhancement pattern. Solid SCAs showed wash-in and wash-out enhancement patterns significantly more often than NF-pNETs ( $P < .05$ ) (Table 2, Figs. 5 and 6).

**3.3. AVR and enhancement patterns performance**

The receiver operating characteristic data curve is shown in Figure 7. AVRs in the unenhanced phase and enhancement patterns showed better performance than AVRs in other phases (Table 3). AUC values of the unenhanced, arterial, portal venous, and delayed phases and enhancement pattern were 0.96 (95% confidence interval [CI], 0.92–1.00), 0.72 (95% CI, 0.58–0.87), 0.80 (95% CI, 0.68–0.92), 0.85 (95% CI, 0.75–0.97), and 0.86 (95% CI, 0.76–0.98), respectively. The best cutoff

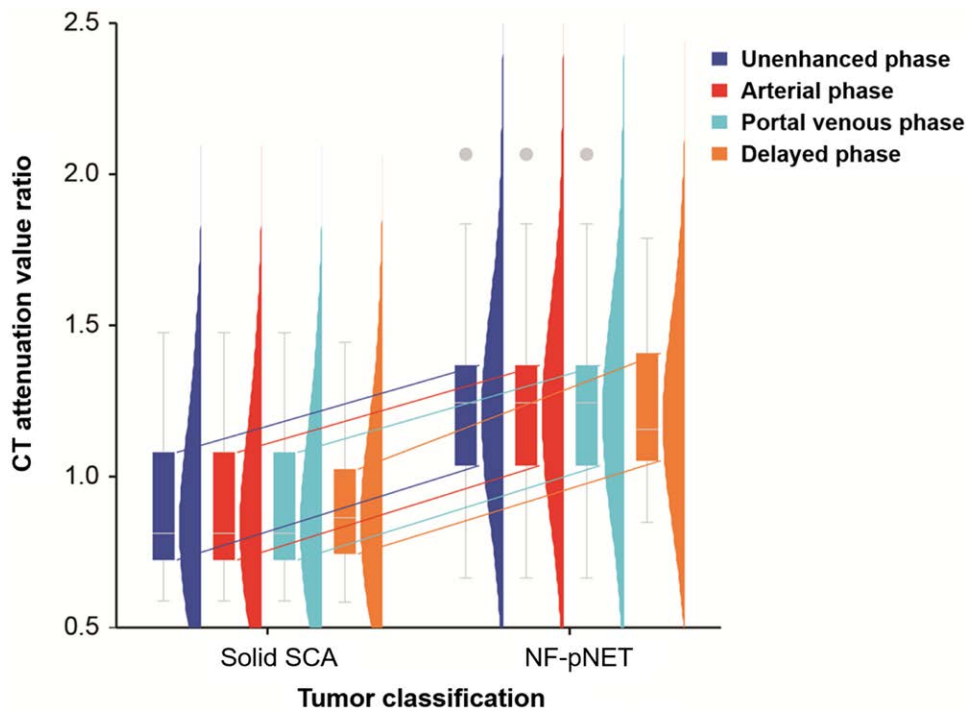


Figure 4. Graph showing the mean attenuation value ratio of solid serous cystadenomas and nonfunctional pancreatic neuroendocrine tumors.

**Table 2**  
CT attenuation value ratio and enhancement pattern in solid serous cystadenomas and nonfunctional pancreatic neuroendocrine tumors.

	Solid SCAs (n = 22)	NF-pNETs (n = 29)	P value
CT attenuation value ratio			
Unenhanced phase	0.59 ± 0.12	0.92 ± 0.13	<.001
Arterial phase	1.10 ± 0.42	1.49 ± 0.60	.007
Portal venous phase	0.90 ± 0.25	1.23 ± 0.31	<.001
Delayed phase	0.90 ± 0.23	1.22 ± 0.22	<.001
Enhancement pattern, n (%)			<.001
Wash-in and wash-out	17 (72.27)	1 (3.45)	
Persistent	5 (22.73)	28 (96.55)	

CT = computed tomography, NF-pNETs = nonfunctional pancreatic neuroendocrine tumors, SCAs = serous cystadenomas.

points based on maximizing sensitivity and specificity sums were 0.77 (sensitivity: 90.91%; specificity: 86.24%; and accuracy: 0.88) in the unenhanced phase, 1.08 (sensitivity: 63.64%; specificity: 75.86%; and accuracy: 0.71) in the arterial phase, 0.99 (sensitivity: 72.73%; specificity: 82.76%; and accuracy: 0.78) in the portal venous phase, and 0.95 (sensitivity: 72.73%; specificity: 93.10%; and accuracy: 0.84) in the delayed phase. Enhancement pattern sensitivity, specificity and accuracy were 96.55%, 77.27% and 0.88%, respectively.

#### 4. Discussion

Solid SCAs AVRs were significantly smaller than NF-pNETs AVRs in all unenhanced, arterial, portal venous, and delayed phases ( $P < .05$ ). Solid SCAs showed wash-in and wash-out enhancement patterns significantly more often than NF-pNETs ( $P < .05$ ). AVR in the unenhanced phase (AUC = 0.96) and enhancement pattern (AUC = 0.96) all showed good performance.

On unenhanced CT, solid SCAs appear as a solid mass with slight low density. Such tumors are called solid SCAs because mass density is approximated as solid density, preventing the tumor minute cystic component from being viewed. Similar to our study, other studies have reported that solid SCAs have lower attenuation values than NF-pNETs on unenhanced CT.<sup>11,17</sup> We found that solid SCAs had the best AUC values in the unenhanced phase compared to the other three contrast-enhanced phases. This may be due to the higher water content in solid SCAs than in NF-pNETs because numerous microcapsules present inside the mass, acting in a manner similar to a “water-absorbing sponge,” rendering these tumors seemingly solid but rich in water, whereas NF-pNETs are absolute solid masses. Previous studies reported that solid SCAs showed a markedly high signal intensity on T2-weighted images and a nonrestrictive pattern on the apparent diffusion coefficient map,<sup>9-11</sup> also explaining the high-water content of solid SCAs.

Due to tight cell packing and the collagen fiber composition observed in solid SCAs and their fibrous septa, which contain abundant capillaries, SCAs are apparently hypervascular and show obvious enhancement on contrast-enhanced CT. This pattern can be easily misdiagnosed as NF-pNET.<sup>11,21</sup> Similar to our study, previous studies have reported that solid SCAs show wash-in and wash-out enhancements.<sup>10,17,18</sup> However, NF-pNETs in our study showed a persistent enhancement pattern. The enhancement degree is dependent on the number of capillaries in the tumor stroma. We speculate that the reasons behind this persistent enhancement pattern were rich tumor stroma and capillaries located in the NF-pNETs. Even though rich tumor stroma and capillaries were observed in solid SCA collagen fibers, they were fewer than those observed in NF-pNETs and only showed significant enhancement in the arterial phase, also possibly explaining why a significant number of solid SCAs had a peak enhanced value in the arterial phase. However, in this study, NF-pNET peak enhanced values in our study were similar to solid SCA enhanced values after matching, rendering the comparison between the 2 enhancement patterns more convincing. Thus, the solid SCA enhancement degree was lower than the normal pancreas enhancement degree in the portal venous and

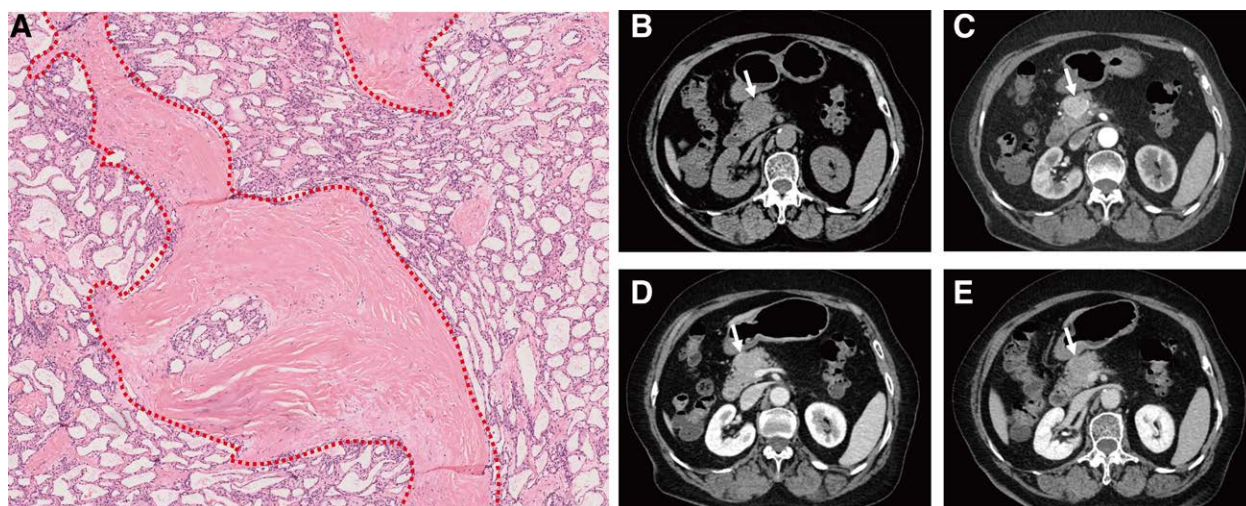


**Figure 5.** Pancreas solid serous cystadenoma in a 70-year-old female patient with abdominal pain. (A) Microscopic examination showed a tumor condensed area with thick fibrous bands and multiple microcysts lined by flat to cuboidal epithelial cells (hematoxylin & eosin, 200 $\times$ ). (B) Unenhanced CT image demonstrating a low-density mass in pancreas head. (C–E) Arterial, portal venous, and delayed phases of contrast-enhanced computed tomography images showing wash-in and wash-out enhancement patterns. CT = computed tomography.

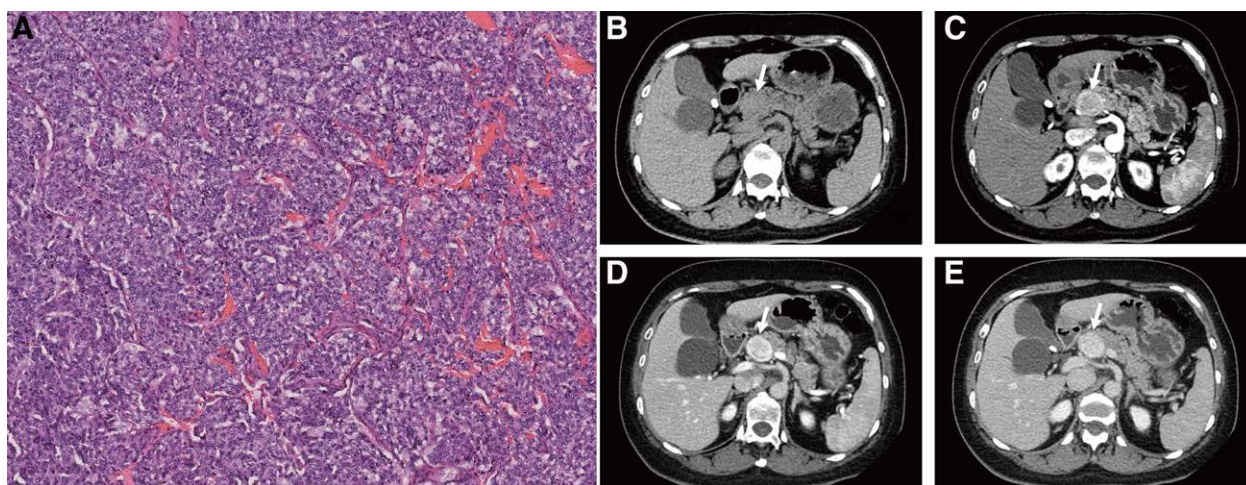


**Figure 6.** Nonfunctional pancreatic neuroendocrine tumor in a 53-year-old male patient with abdominal pain. (A) Microscopic examination shows a well-differentiated neuroendocrine tumor with highly vascular areas (hematoxylin & eosin, 200 $\times$ ). (B) Unenhanced CT image demonstrating a slightly low-density mass in the pancreas head. (C–E) Arterial, portal venous, and delayed phases of contrast-enhanced computed tomography images showing persistent enhancement patterns. CT = computed tomography.

delayed phases, and this was an important CT imaging feature for differentiating NF-pNETs from solid SCAs.

Currently, only 3 original research papers have reported the differential diagnosis of solid SCAs and pNETs by imaging.<sup>[9,11,17]</sup> However, these studies had a small number of patients analyzed by CT. In this study, considering the fact that observational studies on the relationship between AVR and enhancement patterns can be confounded by numerous baseline clinical and CT characteristics, our study sought to address covariate imbalance using PSM, which reduced the imbalance to draw more suitable conclusions. PSM may be more appealing than conventionally including confounders in a regression model because it enables a more intuitive exposure effect analysis between 2 comparable groups. After PSM, AUC values of the unenhanced, arterial, portal venous, and delayed phases and enhancement pattern were 0.96, 0.72, 0.80, 0.85, and 0.86, respectively. In this study, we have included several major clinical and CT imaging factors by PSM that affect the treatment outcome. Other factors such as laboratory indicators,

patient condition, and surgeons experience, which may affect the treatment outcome were not included and hidden bias may actually exist. Therefore, more factors will be included for PSM in the future study.

There are several limitations to this study. First, this was a retrospective study. Second, because we exclude all cystic NF-pNETs and included only surgically resected solid NF-pNETs in our study, the study population cannot reflect all tumors. Third, patients with solid SCAs were evaluated using only CT and not MRI. We will evaluate solid SCA MRI features in a future study. Fourth, we did not evaluate the hemorrhage in the tumor. On one hand, SCAs with hemorrhage is very rare and CT is less sensitive to hemorrhage than MRI, unless there is massive hemorrhage in the tumor. On the other hand, some patients with NF-pNETs and solid SCAs in our study underwent laparoscopic surgery. The tumor specimen was fragmented, and cystic fluid was lost. The pathologist was unable to accurately diagnose hemorrhage. Finally, the findings obtained from the small population may not represent all solid

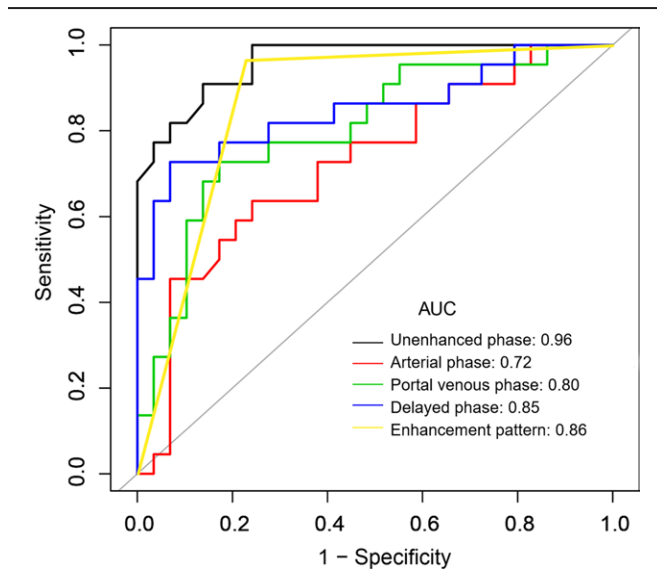


Figure 7. Receiver operating characteristic curve analysis.

**Table 3**  
Apparent performance of CT attenuation values ratio and enhancement pattern.

	AUC (95%CI)	Best threshold	Sensitivity (%)	Specificity (%)	Accuracy
Unenhanced phase	0.96 (0.92, 1.00)	0.77	90.91	86.24	0.88
Arterial phase	0.72 (0.58, 0.87)	1.08	63.64	75.86	0.71
Portal venous phase	0.80 (0.68, 0.92)	0.99	72.73	82.76	0.78
Delayed phase	0.85 (0.75, 0.97)	0.95	72.73	93.10	0.84
Enhancement pattern	0.86 (0.76, 0.98)	—	96.55	77.27	0.88

— = none, AUC = area under the curve, CI = confidence interval, CT = computed tomography.

SCA imaging features; accordingly, we will continue to investigate more patients.

**5. Conclusions**

In conclusion, a low AVR on unenhanced CT and wash-in and wash-out enhancement patterns were useful for differentiating solid SCAs from NF-pNETs and these may be useful for making decisions in clinical settings.

**Author contributions**

**Conceptualization:** Xu Fang.  
**Data curation:** Xu Fang, Hui Jiang.  
**Formal analysis:** Xu Fang.

**Methodology:** Xu Fang, Kai Cao, Jing Li, Fang Liu.  
**Validation:** Li Wang, Jianping Lu, Chengwei Shao.  
**Writing – original draft:** Xu Fang.  
**Writing – review & editing:** Xu Fang, Yun Bian.

**References**

- [1] Chu LC, Singhi AD, Haroun RR, et al. The many faces of pancreatic serous cystadenoma: radiologic and pathologic correlation. *Diagn Interv Imag.* 2017;98:191-202.
- [2] Reid MD, Choi HJ, Memis B, et al. Serous Neoplasms of the pancreas: a clinicopathologic analysis of 193 cases and literature review with new insights on macrocystic and solid variants and critical reappraisal of so-called “Serous Cystadenocarcinoma”. *Am J Surg Pathol.* 2015;39:1597-610.
- [3] Yadav S, Sharma P, Zakalik D. Comparison of demographics, tumor characteristics, and survival between pancreatic adenocarcinomas and pancreatic neuroendocrine tumors: a population-based study. *Am J Clin Oncol.* 2018;41:485-91.
- [4] European Study Group on Cystic Tumours of the Pancreas. European evidence-based guidelines on pancreatic cystic neoplasms. *Gut.* 2018;67:789-804.
- [5] van Huijgevoort NCM, Del Chiaro M, Wolfgang CL, et al. Diagnosis and management of pancreatic cystic neoplasms: current evidence and guidelines. *Nat Rev Gastroenterol Hepatol.* 2019;16:676-89.
- [6] Scott AT, Howe JR. Evaluation and management of neuroendocrine tumors of the pancreas. *Surg Clin North Am.* 2019;99:793-814.
- [7] Matsubayashi H, Matsui T, Yabuuchi Y, et al. Endoscopic ultrasonography guided-fine needle aspiration for the diagnosis of solid pancreaticobiliary lesions: clinical aspects to improve the diagnosis. *World J Gastroenterol.* 2016;22:628-40.
- [8] Lee YN, Moon JH, Kim HK, et al. A triple approach for diagnostic assessment of endoscopic ultrasound-guided fine needle aspiration in pancreatic solid masses and lymph nodes. *Dig Dis Sci.* 2014;59:2286-93.
- [9] Jang KM, Kim SH, Song KD, et al. Differentiation of solid-type serous cystic neoplasm from neuroendocrine tumour in the pancreas: value of abdominal MRI with diffusion-weighted imaging in comparison with MDCT. *Clin Radiol.* 2015;70:153-60.
- [10] Chen JY, Chen HY, Pan Y, et al. Computed tomography and magnetic resonance imaging features of solid serous cystadenomas of the pancreas. *Oncol Lett.* 2019;18:898-906.
- [11] Park HS, Kim SY, Hong SM, et al. Hypervascular solid-appearing serous cystic neoplasms of the pancreas: differential diagnosis with neuroendocrine tumours. *Eur Radiol.* 2016;26:1348-58.
- [12] Kuss O, Blettner M, Borgermann J. Propensity score: an alternative method of analyzing treatment effects. *Dtsch Arztebl Int.* 2016;113:597-603.
- [13] Staffa SJ, Zurakowski D. Five steps to successfully implement and evaluate propensity score matching in clinical research studies. *Anesth Analg.* 2018;127:1066-73.
- [14] Szczykutowicz TP, DuPlissis A, Pickhardt PJ. Variation in CT number and image noise uniformity according to patient positioning in MDCT. *AJR Am J Roentgenol.* 2017;208:1064-72.
- [15] Skrzynski W, Zielinska-Dabrowska S, Wachowicz M, et al. Computed tomography as a source of electron density information for radiation treatment planning. *Strahlenther Onkol.* 2010;186:327-33.
- [16] Arends MJ, Masashi F, Klimstra D, et al. WHO Classification of Tumours of the Digestive System. 5 ed. Lyon, France: IARC Press; 2019:303-5.
- [17] Hayashi K, Fujimitsu R, Ida M, et al. CT differentiation of solid serous cystadenoma vs endocrine tumor of the pancreas. *Eur J Radiol.* 2012;81:e203-8.
- [18] Katsourakis A, Dimitriou I, Noussios G, et al. Solid serous adenoma of the pancreas: a case report and review of the literature. *Case Rep Surg.* 2016;2016:3730249.